Spin glass behaviour of amorphous Ge–Mn alloy thin films

2007 J. Phys.: Condens. Matter 19 036211

(http://iopscience.iop.org/0953-8984/19/3/036211)

INSTITUTE OF PHYSICS PUBLISHING JOURNAL OF PHYSICS: CONDENSED MATTER

J. Phys.: Condens. Matter **19** (2007) 036211 (10pp) doi:10.1088/0953-8984/19/3/036211

Spin glass behaviour of amorphous Ge–Mn alloy thin films

S H Song[1], M H Jung[2] and S H Lim[3,4]

[1] Materials Science and Engineering, Iowa State University, Ames, IA 50011-3020, USA
[2] Quantum Material Research Team, Korea Basic Science Institute, 52 Yeoeun-dong, Yusung-gu, Daejeon 305-333, Korea
[3] Department of Materials Science and Engineering, Korea University, Anam-dong, Seongbuk-gu, Seoul 136-713, Korea

E-mail: sangholim@korea.ac.kr

Received 29 July 2006, in final form 7 December 2006
Published 5 January 2007
Online at stacks.iop.org/JPhysCM/19/036211

Abstract

Magnetic measurements are performed under ac and dc conditions on well characterized $Ge_{100-x}Mn_x$ (x in at.%) amorphous thin films prepared by thermal co-evaporation onto oxidized Si or glass substrates at room temperature. M–H hysteresis loops at 5 K show that saturation does not occur even at a high applied field of 30 or 50 kOe. The temperature dependence of the dc and ac susceptibility shows a cusp with a position and magnitude that vary with the frequency during the ac susceptibility measurements. These results suggest a spin glass behaviour at low temperatures. Two competing magnetic interactions between Mn ions, which are responsible for the spin glass behaviour, are considered to be the direct antiferromagnetic coupling and the indirect ferromagnetic coupling through conduction electrons or holes. Scaling analysis indicates that the indirect ferromagnetic interactions are long range.

1. Introduction

The existence of a spin glass phase in II–VI diluted magnetic semiconductors (DMSs) doped with Mn ions has been well documented in the literature [1–7]. Well known examples include CdMnTe [1–3], PbMnTe [4], HgMnTe [5], ZnMnTe [6], and SnMnTe [7]. These alloys are crystalline compounds. However, these compounds have an amorphous structure from the 'magnetic' point of view. This is because Mn ions, which are the only magnetic elements, *randomly* fill the fcc sublattice sites formed within the compound structure. This means disordered magnetic doping in an otherwise regular host lattice. With the exception of SnMnTe, the bandgap in these materials is relatively large (∼1 eV). Therefore, the carrier concentration (electrons or holes) is small. This indicates that the indirect carrier-mediated

[4] Author to whom any correspondence should be addressed.

exchange interactions (also known as modified RKKY interactions) in these compounds are quite weak or even absent. Therefore, the dominant exchange interactions among Mn ions are antiferromagnetic and are direct and short ranged, usually between the nearest neighbours and next-nearest neighbours. In this type of II–VI DMSs, the frustration, the origin of a spin glass behaviour, occurs among the antiferromagnetically coupled Mn ions [8].

Another class of DMSs showing a spin glass behaviour is amorphous alloys containing magnetic ions [9–12], which is the subject of this investigation. In this case, magnetic ions are certainly randomly distributed due to structural randomization. From the viewpoint of a random distribution of magnetic elements, this type of amorphous DMSs is similar to that of II–VI DMSs. However, there are many differences resulting from the structural randomization, with one notable example being electrical conductivity [8]. The conduction electron elastic mean free path is reduced significantly by the amorphous nature of the material, which is the reason behind the significantly higher dopant concentration near the metal–insulator transition in these alloys. The dopant concentration in amorphous alloys needed to reach the metal–insulator transition ($\sim 10^{21}$ cm^{-3}) is many orders of magnitude larger that that in crystalline materials ($\sim 10^{17}$ cm^{-3}) [13]. A similar difference exists in the carrier concentration. In spintronics (spin-based electronics or spin electronics) applications where the DMSs are mainly used to inject spins into semiconductors without being hampered by a mismatch in conductivity, the carrier concentration needs to be near the metal–insulator transition [14–16]. Therefore, amorphous DMSs suitable for spintronic applications need to have a high density of carriers. However, these carriers are localized due to structural randomization [10]. This localization is further facilitated by large Coulombic carrier–carrier interactions as a result of the high density of carriers and carrier–local moment interactions [10]. Although the carriers are localized, the localization length is rather long, and not confined to the atomic scale [10]. Therefore, unlike II–VI DMSs, there are indirect RKKY interactions in amorphous DMSs, which are mainly ferromagnetic coupling. With the presence of two opposite couplings in amorphous DMSs, direct antiferromagnetic and indirect ferromagnetic RKKY interactions, the frustration can be due to competition between these two couplings.

In this work, the spin glass behaviour of amorphous Ge–Mn thin films is investigated. Recently, group-IV-based DMSs have attracted significant attention, due to the prediction of a high Curie temperature from theory based on the Zener model [17]. Among the many group IV semiconductors, Ge has received the most attention [18–20]. Ge has an important advantage in that it is lattice matched to the AlGaAs/GaAs family, which facilitates incorporation into III–V heterostructures. Furthermore, Ge has a higher intrinsic hole mobility than either GaAs or Si. The results reported on group-IV-based DMSs thus far are encouraging, with the most significant results being observed by Park *et al* in epitaxial Ge–Mn thin films deposited by MBE [18]. Ferromagnetic ordering with reasonably high Curie temperatures has been reported. In addition, voltage-controlled ferromagnetic order was demonstrated with a low gate voltage of 0.5 V, which has opened up the possibility of new spintronic devices. However, the highest Curie temperature achieved thus far is 116 K, which is the largest impediment to widespread applications in spintronics. The main reason for the low Curie temperature might be the limited Mn content incorporated into Ge. Recent first principles calculations predict that the Mn–Mn exchange interactions, and hence the Curie temperature, can be increased by increasing the Mn content [21]. However, the introduction of Mn into Ge was found to be very limited, with the highest amount of Mn incorporated without segregation being 3.3 at.% even with a very low temperature (70 °C) MBE process [18].

Higher Curie temperatures were reported in Mn-doped Ge bulk single crystals [19]. The maximum amount of Mn introduced in Ge without forming a secondary phase was claimed to be 6.2% and the Curie temperature was reported to be as high as 285 K at this Mn content,

which is reasonably close to room temperature. However, the reported high Mn content in Ge bulk crystals is questionable considering that the terminal solubility of Mn in Ge is extremely small [22] and the Mn-doped Ge crystals were fabricated under conditions close to equilibrium [19]. It is well known that the terminal solubility increases as the metastability of the system increases. This is precisely the reason why, in earlier works [18, 20, 23], the LTMBE process was used to increase the metastability and hence Mn solubility.

An ultimate increase in metastability can be realized by forming an amorphous phase. With the formation of an amorphous phase, it is expected that a large amount of Mn can be incorporated into Ge without forming second phases, possibly leading to a high Curie temperature. Indeed, ferromagnetic ordering has been observed at room temperature in well characterized $Ge_{100-x}Mn_x$ (x in at.%) amorphous thin films over a wide composition range [24]. Potentially, this is of significant practical importance in spintronics. More scattering centres are expected to exist in amorphous thin films than in crystalline counterparts, possibly leading to shorter spin flip length. Therefore, more work needs to be done in the future including measurements of spin polarization. From a theoretical point of view, it is important to understand the magnetic behaviour of Ge–Mn alloys containing a large number of magnetic Mn ions, which was the main purpose of this study.

Very recently, works on amorphous Ge–Mn alloy thin films were reported by Yu *et al* [25] and Verna *et al* [26]. The thin films were fabricated either by thermal evaporation [25] or ion implantation [26]. Magnetic and Hall measurements for the evaporated thin films indicate that the ferromagnetic/paramagnetic transition occurs at 150 K [25]. On the other hand, the magnetic properties of the implanted thin films were found to be poor, the Curie temperature being approximately 20 K. In both cases, no investigation was carried out to examine a spin glass behaviour of these magnetic thin films.

2. Experimental method

$Ge_{100-x}Mn_x$ (x in at.%) thin films with a typical thickness of 100 nm were prepared by thermal co-evaporation onto an oxidized Si substrate at room temperature. The thickness of the SiO_2 was 100 nm (0.1 μm) and that of Si was 200 μm. The base pressure was $<2 \times 10^{-6}$ Torr. The film thickness was measured using a profilometer. Phase analysis was carried out by x-ray diffraction (XRD) with Cu Kα radiation and high-resolution transmission electron microscopy (HRTEM). The composition was determined by Rutherford backscattering (model number 6SBH2, National Electrostatic Corporation, USA) with a beam of 2 MeV He ions. A superconducting quantum interference device (SQUID) and an alternating gradient magnetometer (AGM) were used for magnetic characterization under static conditions. The magnetic susceptibility under ac conditions was measured using a physical property measurement system (PPMS) over a wide frequency range of 0.1–10 kHz. The magnetic measurements were carried out down to LH temperature.

3. Results and discussion

Systematic experiments of XRD and HRTEM were carried out to characterize the microstructure of the thin films. The microstructural results indicate the formation of a single amorphous phase up to $x \approx 40$, above which a crystalline phase precipitates with an unidentified face-centred cubic symmetry [24].

The magnetization versus temperature (M–T) data, measured under the zero-field-cooled conditions over a temperature range from 4 to 300 K at an applied magnetic field of 15 kOe, does not show the usual Brillouin behaviour, which is characterized by the slow

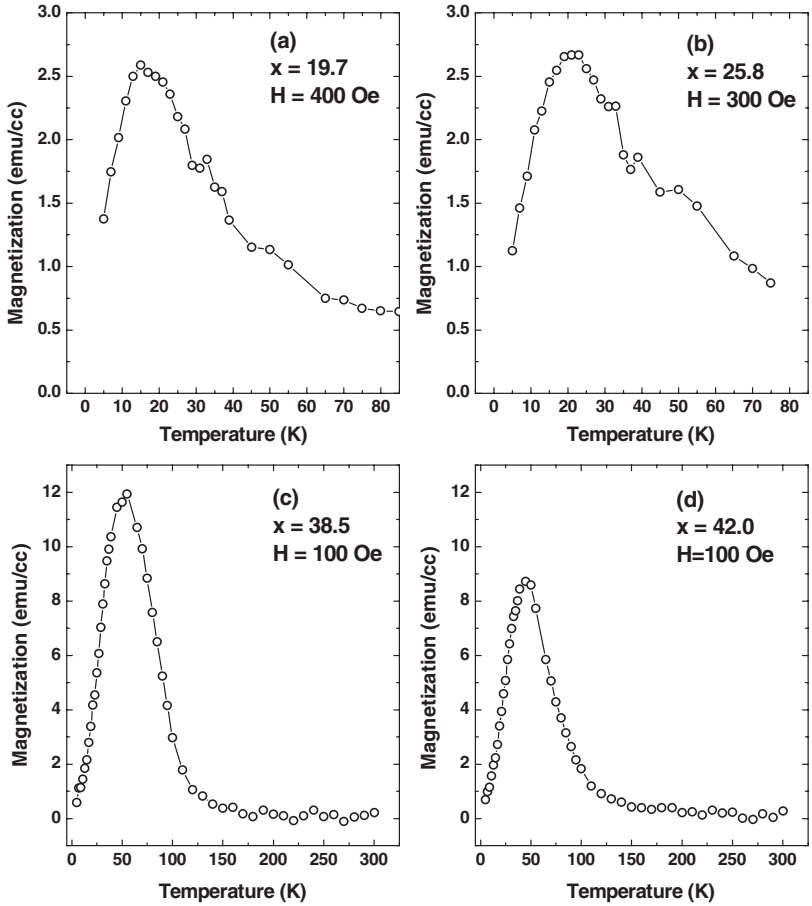

Figure 1. M–T curves for $Ge_{100-x}Mn_x$ thin films with various Mn contents measured with a SQUID over a temperature range from 4 to 300 K. The results were obtained under the zero-field-cooled condition and at a small applied field ranging from 100 to 400 Oe. (a) $x = 19.7$, (b) $x = 25.8$, (c) $x = 38.5$, and (d) $x = 42.0$.

decrease in magnetization at low temperatures followed by an abrupt decrease near the Curie temperature. Instead, the present M–T curves show a significant decrease in magnetization in the low temperature range with increasing temperature, followed by a rather slow decrease in magnetization at higher temperatures [24]. This temperature dependence results in an unusual concave shape of the M–T curve. Despite this unusual behaviour, there is a monotonic decrease in magnetization with increasing temperature. However, this monotonic decrease in magnetization with increasing temperature was not observed in the M–T curves measured at relatively low applied fields (100–400 Oe), as shown in figures 1(a)–(d) for the samples with various compositions, $x = 19.7$, 25.8, 38.5, and 42.0, respectively. The M–T curves show a cusp; i.e., magnetization initially increases with increasing temperature, reaching a maximum and then decreasing with further increases in temperature. This type of cusp-shaped M–T curves is most likely to be associated with a spin glass behaviour. The temperature at which the broad peak occurs depends on x and tends to increase with increasing x, even though the maximum occurs at $x = 38.5$ where the peak temperature is 54 K. This peak temperature is significantly larger than the 15 K observed at $x = 19.7$.

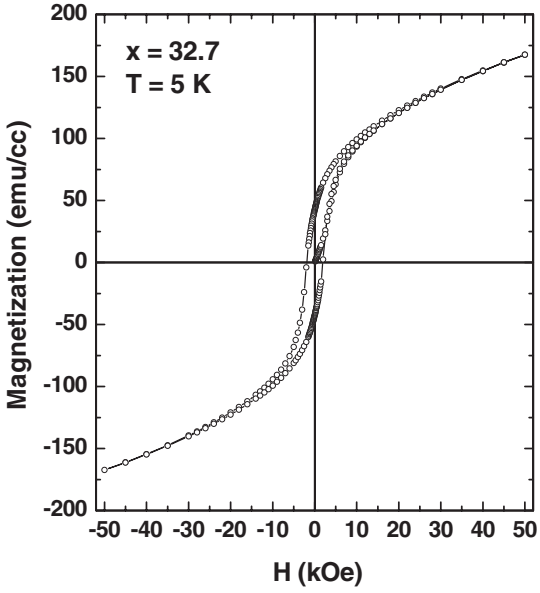

Figure 2. M–H hysteresis loops measured with a SQUID at 5 K for the sample with $x = 32.7$.

Cusp-shaped M–T curves are often observed in superparamagnetic systems, in which the cusp is known as the blocking temperature, indicating a transition from the superparamagnetic into the ferromagnetic state. However, the possibility of superparamagnetism can be ruled out with the present microstructure of a single amorphous phase because superparamagnetism is usually related to the formation of small magnetic clusters with a magnetic anisotropy energy comparable to the thermal energy. One possible reason for the observed M–T curves can be the significant increase in single ion anisotropy in the low temperature range, as was observed in amorphous RE–TM (where RE and TM stand for the rare earths and 3d transition metals, respectively) alloys [27]. Since the anisotropy of a single ion RE is randomly distributed in amorphous RE–TM alloys, the magnetization at a small applied field will decrease with increasing anisotropy at low temperatures. However, this possibility can again be ruled out because the M–H curves measured at a low temperature of 5 K do not show saturation even at a very high applied field of 30 or 50 kOe (see figure 2 for $x = 32.7$, as an example). Under the present conditions (a temperature of 5 K and an applied field of 30 or 50 kOe), the Zeeman energy is much higher than the thermal energy, resulting in the complete saturation in a normal situation, including the case of an amorphous RE–TM alloy with a very high single ion anisotropy [27]. Furthermore, Mn ions have a much smaller single ion anisotropy than rare earths.

The unsaturated spin state even at a very high Zeeman to thermal energy ratio suggests a spin glass phase below the peak temperature. In the concentration range examined in this study, $\sim 10 < x < \sim 40$, the Hall measurements show a large level of carrier concentration, being 10^{20}–10^{21} cm^{-3}, even though the type and magnitude depend on the Mn content and temperature [24]. Therefore, as discussed in section 1, two competing magnetic interactions are considered to be operating between Mn ions; one being direct antiferromagnetic coupling and the other indirect ferromagnetic coupling mediated through conduction electrons or holes (RKKY interaction). Usually, antiferromagnetic coupling is expected to be stronger than the ferromagnetic interaction. However, in this case, ferromagnetic coupling is also considered to be strong in the presence of a large carrier concentration. Because of these two competing

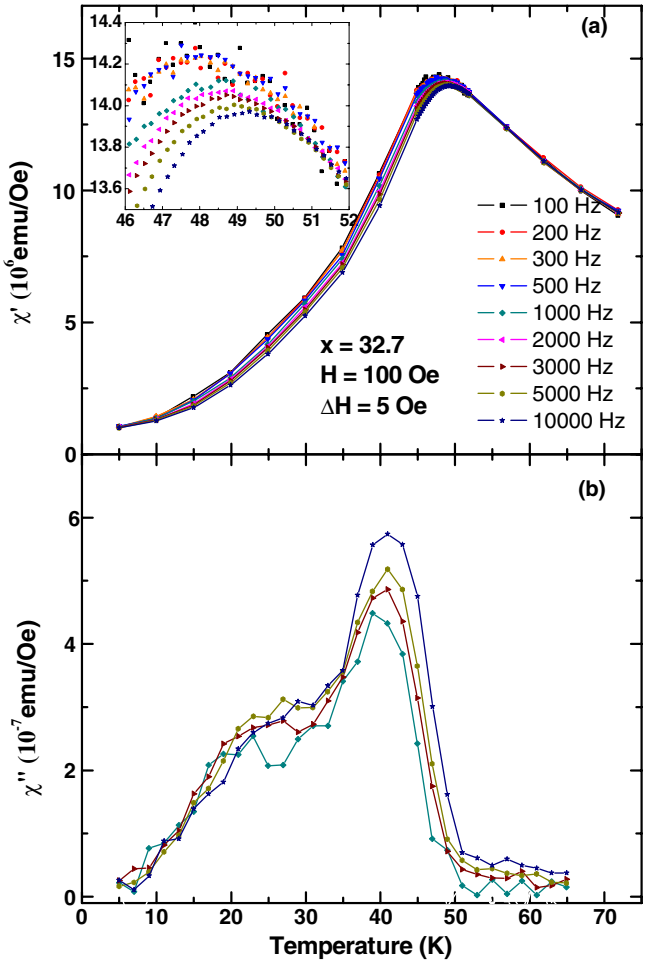

Figure 3. The temperature dependence of (a) the real part and (b) the imaginary part of the ac susceptibility for the sample with $x = 32.7$ at various frequencies (100, 200, 300, 500, 1000, 2000, 3000, 5000, and 10 000 Hz). During the measurements, a constant dc bias field of 100 Oe was applied and the amplitude of the ac field was 5 Oe. The inset shows the magnified parts near the spin freezing temperature.

(This figure is in colour only in the electronic version)

antiferromagnetic and ferromagnetic interactions as well as the random distribution of Mn ions, the magnetic state can easily be 'frustrated', leading to a spin glass state.

In order to confirm the spin glass state, the temperature dependence of the ac susceptibility was measured over a wide frequency range from 100 Hz to 10 kHz. Both the real (in-phase component, χ') and imaginary (out-of-phase component, χ'') parts of the susceptibility were measured, and the results are shown in figures 3(a) and (b), respectively, for the sample with $x = 32.7$. The inset shows the magnified results near the spin freezing temperature (T_f) to highlight the frequency dependence of the in-phase susceptibility near T_f. During the measurements, a constant dc bias field of 100 Oe was applied and the amplitude of the ac field was fixed to 5 Oe. There is little scatter in the measured data of the in-phase component except under low measured frequencies (below 500 Hz) near the peak, as can be seen clearly

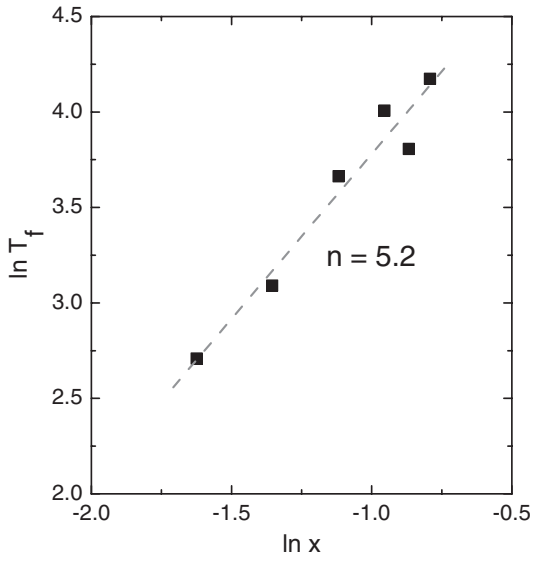

Figure 4. $\ln T_f$ versus $\ln x$ plots used to determine the exponent n for $J(R) = J_0 R^{-n}$.

from the inset in figure 3(a). However, in the case of out-of-phase component data, there is large scatter over the whole temperature and frequency ranges, which is possibly due to much smaller magnitude of the signal. Note that the y-axis scale of the out-of-phase component is much smaller than that of the in-phase component. In particular, the scatter of the out-of-phase data at low frequencies of 500 Hz and below are quite large, and are not shown in figure 3(b). A clear difference in the temperature dependence of the susceptibility as a function of the measured frequency was observed, as shown in the magnified part shown in the inset. In the case of the in-phase component (figure 3(a)), the susceptibility is highest (lowest) at the lowest (highest) measured frequency. The opposite is true for the imaginary part of the susceptibility (figure 3(b)). The cusps, which are characteristic of spin freezing, can be clearly seen in the figures. The magnitude and position of the cusp vary continuously with the frequency. The peak value of the in-phase component decreases with increasing frequency while that of the out-of-phase component increases. However, the position of the peak shifts toward the high temperature region with increasing frequency in both cases. It should be noted that that the susceptibility profiles differ substantially over the whole temperature range depending on the measured frequency, except for the in-phase component above T_f.

T_f can be obtained from the temperature dependence of the dc (figures 1(a)–(d)) or ac susceptibility measured at various frequencies (figures 3(a) and (b)). In this study, T_f was obtained from the dc data. With increasing x, the T_f increases from 15 K at $x = 19.7$ to 65 K at $x = 45.3$. Scaling analysis was developed to estimate the exponent (n), which describes the range of ferromagnetic interactions between Mn ions mediated by carriers [28]. Scaling analysis exploits the fact that, for a continuous and random distribution of magnetic ions, exactly the case of the present system, $(R_{ij})^3$ (x) is constant, where R_{ij} denotes the separation between the magnetic ions (Mn ions in this case). The following relation between T_f and x was developed from the scaling analysis: $\ln T_f \sim (n/3) \ln x$ [28]. It is clear from the relation that the magnitude of n can be obtained from the slope of $\ln T_f$ versus $\ln x$, which is shown in figure 4 for the present Ge–Mn system. The value of n was calculated to be approximately 5.2, indicating that the radial dependence of the exchange interaction between Mn ions varies as $J(R) \sim R^{-5.2}$. It should be noted that $n = 5$ has been observed for narrow

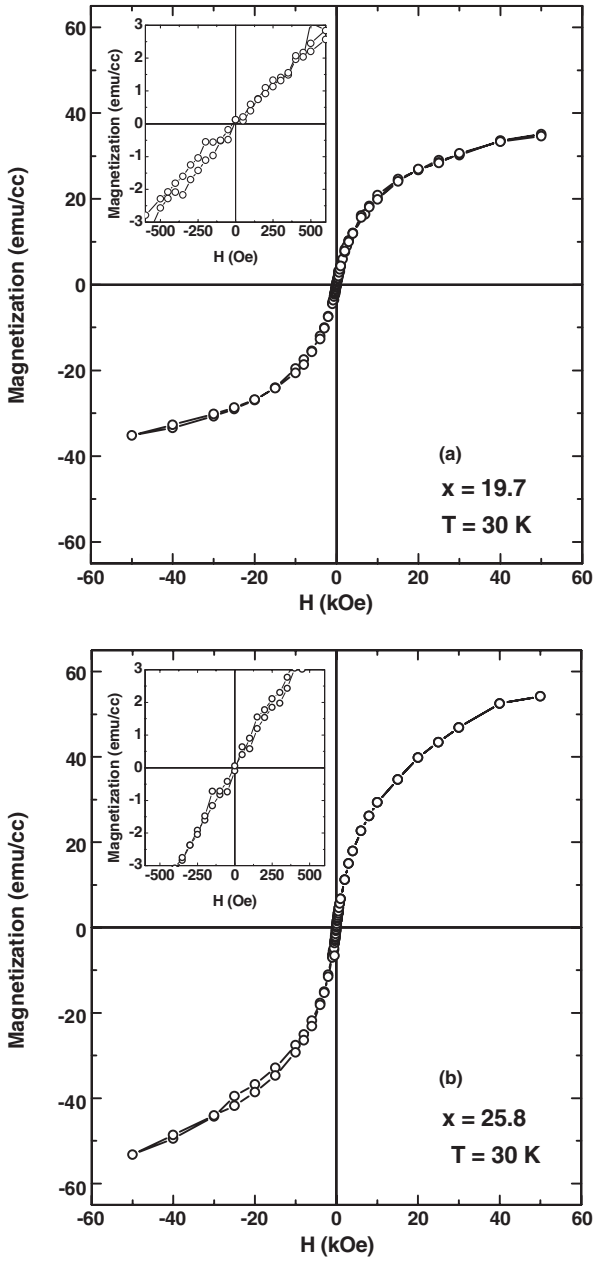

Figure 5. The M–H curves measured with a SQUID at 30 K for the samples of (a) $x = 19.7$ and (b) $x = 25.8$. The spin freezing temperature is 15 K at $x = 19.7$ and 21 K at $x = 25.8$. In each figure, the magnified part near the origin is also shown in the inset. The loop at $x = 25.8$ is open at large applied fields, which is possibly due to the drift during the measurement. In order to better compare the magnetization between the samples, the y-axis scales of the two figures are identical to each other.

bandgap DMSs such as (Hg, Mn)Te and (Hg, Mn)Se [28]. The magnitude of n in these Ge–Mn thin films as well as for narrow bandgap DMSs is small in magnitude, indicating that the

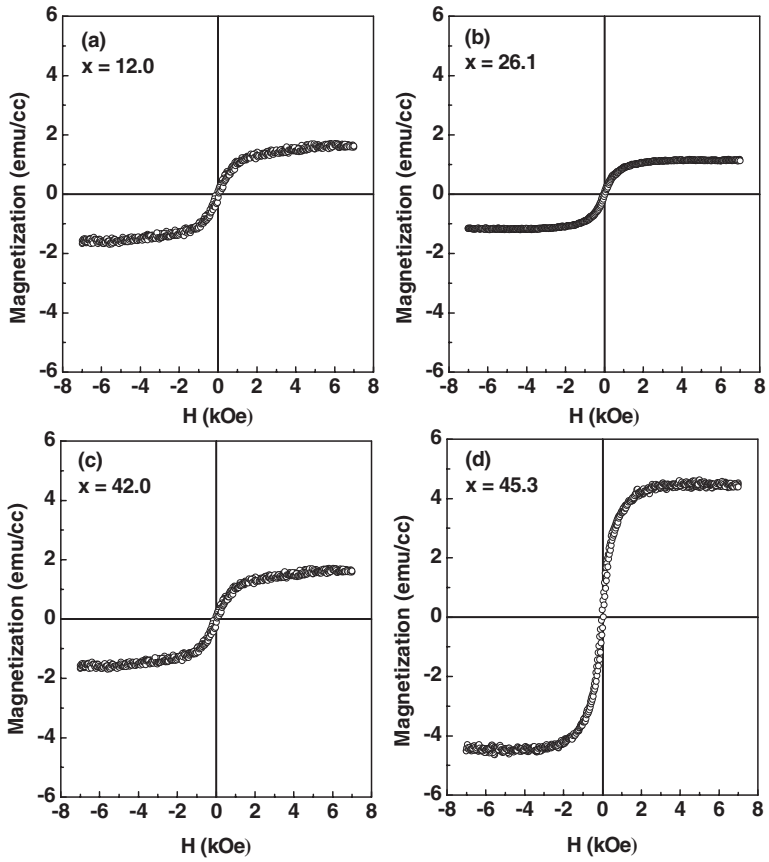

Figure 6. The M–H loops measured with an AGM at room temperature for various samples with (a) $x = 12.0$, (b) $x = 26.1$, (c) $x = 42.0$, and (d) $x = 45.3$. In order to better compare the magnetization between the samples, the y-axis scales of all the figures are identical to each other.

ferromagnetic exchange interactions between Mn ions are long range. This can be understood from the fact that both amorphous Ge–Mn thin films and the narrow bandgap DMSs have a large carrier concentration, which facilitates long ranged indirect ferromagnetic RKKY interactions mediated by the carriers.

It is of interest to know the magnetic state above the spin freezing temperature. In an effort to understand this, M–H loops were measured above the spin freezing temperatures. The M–H curves at 30 K (just above the spin freezing temperature), measured with a SQUID, are shown in figures 5(a) and (b) for the samples with $x = 19.7$ and 25.8, respectively. Note that the spin freezing temperature is approximately 15 K at $x = 19.7$ and 22 K at $x = 25.8$. The room temperature hysteresis loops measured with an AGM are shown in figures 6(a)–(d) for various samples with $x = 12.0$, 26.1, 42.0, and 45.3, respectively. The most prominent features common to the results shown in figures 5 and 6 are the zero coercivity and lack of remanence, namely, non-hysteretic behaviour. The magnified parts shown in the insets of figures 5(a) and (b) clearly show this feature at 30 K. However, there is also some difference in the results obtained at the two different temperatures. At 30 K, the saturation is not reached even at the highest field of 50 kOe. However, this is not the case at room temperature, a clear saturation occurring at 1–2 kOe.

4. Conclusions

Amorphous semiconducting $Ge_{100-x}Mn_x$ (x in at.%) thin films were prepared by thermal co-evaporation onto oxidized Si or glass substrates at room temperature. Microstructural characterization by XRD and HRTEM indicated the formation of a single amorphous phase up to $x \approx 40$. Detailed magnetic measurements including the M–T curves at moderately small applied fields and the temperature dependence of the ac susceptibility over a wide frequency range suggest the thin films to have a spin glass behaviour. This can be understood from the two competing magnetic interactions between Mn ions: the direct antiferromagnetic coupling and indirect ferromagnetic coupling through conduction electrons or holes (RKKY interaction). Indirect ferromagnetic coupling is considered to be strong with the presence of a large carrier concentration of 10^{20}–10^{21} cm^{-3} obtained from the Hall measurements. Scaling analysis showed that the indirect ferromagnetic interactions mediated by carriers were long range, which was expected from the large carrier concentration.

Acknowledgments

This work was supported by the Korean Ministry of Science and Technology through the National Research Laboratory programme. Work at KBSI was supported in part by the Korean Ministry of Commerce, Industry and Energy.

References

[1] Mauger A, Villian J, Zhou Y, Rigaux C, Bontemps N and Ferre J 1990 *Phys. Rev.* B **41** 4587
[2] Geschwind S, Huse D A and Devlin G E 1990 *Phys. Rev.* B **41** 4854
[3] Bertrand D, Mauger A, Ferre J and Beauvillain P 1992 *Phys. Rev.* B **45** 507
[4] Tholence J L, Benoit A, Mauger A, Escorne M and Triboulet R 1984 *Solid State Commun.* **49** 417
[5] Zhou Y, Rigaux C, Mycielski A, Menant M and Bontemps N 1989 *Phys. Rev.* B **40** 8111
[6] Shand P M, Christianson A D, Pekarek T M, Martinson L S, Schweitzer J W, Miotkowski I and Crooker B C 1998 *Phys. Rev.* B **58** 12876
[7] Escorne M, Godinho M, Tholence J L and Mauger A 1985 *J. Appl. Phys.* **57** 3424
[8] Binder K and Young A P 1986 *Rev. Mod. Phys.* **58** 801
[9] Hellman F, Tran M Q, Gebala A E, Wilcox E M and Dynes R C 1996 *Phys. Rev. Lett.* **77** 4562
[10] Zink B L, Janod E, Allen K and Hellman F 1999 *Phys. Rev. Lett.* **83** 2266
[11] Hellman F, Queen D R, Potok R M and Zink B L 2000 *Phys. Rev. Lett.* **84** 5411
[12] Zink B L, Preisler V, Queen D R and Hellman F 2002 *Phys. Rev.* B **66** 195208
[13] Furdyna J K 1982 *J. Appl. Phys.* **53** 7637
[14] Smith D L and Silver R N 2001 *Phys. Rev.* B **64** 045323
[15] Albrecht J D and Smith D L 2002 *Phys. Rev.* B **66** 113303
[16] Albrecht J D and Smith D L 2003 *Phys. Rev.* B **68** 035340
[17] Dietl T, Ohno H, Matsukura F, Cibert J and Ferrand D 2000 *Science* **287** 1019
[18] Park Y D, Hanbicki A T, Erwin S C, Hellberg C S, Sullivan J M, Mattson J E, Ambrose T, Wilson A, Spanos G and Jonker B T 2002 *Science* **295** 651
[19] Cho S, Choi S, Hong S C, Kim Y, Ketterson J B, Kim B J, Kim Y C and Jung J H 2002 *Phys. Rev.* B **66** 033303
[20] Kioseoglou G, Hanbicki A T, Li C H, Erwin S C, Goswami R and Jonker B T 2004 *Appl. Phys. Lett.* **84** 1725
[21] Zhao Y J, Shishidou T and Freeman A J 2003 *Phys. Rev. Lett.* **90** 047204
[22] Massalski T B 1990 *Binary Alloy Phase Diagrams* (Metals Park, OH: American Society for Metals) p 1964
[23] Ohno H, Shen A, Matsukura F, Oiwa A, Endo A, Katsumoto S and Iye Y 1996 *Appl. Phys. Lett.* **69** 363
[24] Song S H, Lim S H, Jung M H, Santos T S and Moodera J S 2006 *J. Korean Phys. Soc.* **49** 2386
[25] Yu S S, Anh T T L, Ihm Y E, Kim D, Kim H, Hong S K, Oh S, Kim C S, Lee H J and Woo B C 2006 *Curr. Appl. Phys.* **6** 545
[26] Verna A, Ottaviano L, Passacantando M, Santucci S, Picozzi P, D'Orazio F, Lucari F, De Biase M, Gunnella R, Berti M, Gasparotto A, Impellizzeri G and Priolo A 2006 *Phys. Rev.* B **74** 085204
[27] Chudnovsky E M 1988 *J. Appl. Phys.* **64** 5770
[28] Twardowski A, Swagten H J M, de Jonge W J M and Demianiuk M 1987 *Phys. Rev.* B **36** 7013